ICARUS 100, 40–47 (1992)

Stability of Polar Frosts in Spherical Bowl-Shaped Craters on Moon, Mercury, and Mars[1]

ANDREW P. INGERSOLL, TOMAS SVITEK, AND BRUCE C. MURRAY

Division of Geological and Planetary Sciences, California Institute of Technology, Pasadena, California 91125

Received June 29, 1982; revised August 13, 1992

Following Svitek (*Martian Water Frost: Control of Global Distribution by Small-Scale Processes*, Ph.D. Thesis, California Institute of Technology, 1992), analytic solutions are presented for the effective albedo, the effective emissivity, and the radiative equilibrium temperature in the shadowed portions of a spherical bowl-shaped crater. The model assumes that the surface is a Lambert scatterer with visual albedo and infrared emissivity each independent of wavelength across their respective spectral ranges. Absorption, emission, and multiple scattering from the walls of the crater are treated rigorously to all orders. For airless bodies whose surfaces are in radiative equilibrium, all shadowed portions of any individual crater have the same temperature, whose value depends on four quantities: the insolation (product of the solar constant and the sine of the solar elevation angle), the depth/diameter ratio of the crater, the visual albedo, and the infrared emissivity. As long as the crater is deep enough to have shadows, the lowest temperatures are for the shallowest craters—those with the smallest depth/diameter ratio. The model is applied first to the Moon and Mercury using a depth/diameter ratio of 0.2, which is typical of the lunar highlands according to Pike (*Geophys. Res. Lett.* 1, 291–294 (1974); in *Impact and Explosion Cratering* (Roddy *et al.*, Eds.), pp. 489–509, Pergamon, New York, 1977). For Mercury and the Moon, temperatures in shadows in polar craters are below 102 K, so the sublimation rate of water ice calculated according to the model of Watson *et al.* (*J. Geophys. Res.* 66, 3033–3015 (1961)) is less than 1 cm per byr. The latitudinal extent of the cold zone on the Moon is greater than that on Mercury, although temperatures at the poles of the two planets are similar. The other application is to polar frosts on Mars. Illuminated water frosts in radiative equilibrium grow rougher, because the average temperature of a depression is greater than that of flat ground. Subliming CO_2 frosts, which are always at the same temperature, grow rougher at low solar elevation angles because the heat flux absorbed by a depression is greater than that for a flat surface. At high insolation rates (high Sun near perihelion) the average heat flux to a depression is less than for a flat surface. The latter evaporates faster, which makes the average surface smoother and leads to a high average albedo. This behavior helps explain the fact that the south CO_2 cap, which receives its greatest insolation near perihelion, has a higher effective albedo and therefore can survive the summer, whereas the north CO_2 cap has a lower effective albedo and disappears each year around summer solstice.

1. INTRODUCTION

The high radar reflectivity of Mercury's north and south poles (Butler *et al.*, 1992; Slade *et al.*, 1992; Harmon and Slade, 1992) is strong evidence for the presence of water ice. As shown by Watson *et al.* (1961), ice could be stable on an airless body provided its temperature was low enough. An upper bound on the loss rate is the sublimation rate into vacuum, which is proportional to the saturation vapor pressure divided by the thermal speed of the molecules. For frost at a temperature of 120 K, Watson *et al.* estimate the maximum loss rate to be 8 m of ice per byr. This rate decreases by a factor of 2 for every 1.6 K drop in temperature. Although the lifetime is uncertain, as is the overall abundance of water on these bodies, the calculations suggest that meter-thick deposits of water ice could be stable for billions of years if the temperature never exceeds 110 to 120 K.

If the solar elevation angle were small enough (i.e., if the Sun is never far above the horizon), water ice would be stable even if the surface were flat. Paige *et al.* (1992) consider a flat surface at the pole of Mercury, assuming the obliquity is essentially zero. Half of the solar disk is above the horizon, and the frost receives light obliquely from this source. Paige *et al.* state that the temperatures of flat surfaces at Mercury's poles are not expected to exceed 167 K where the albedo A is low. Temperatures below 120 K occur for $A = 0.75$. They also state that significantly colder temperatures are expected within the permanently shadowed portions of impact craters, citing a model by Adorjan (1970), Hodges (1980), and Svitek (1992) in which the interior surfaces of craters are repre-

[1]Contribution number 5186 from the Division of Geological and Planetary Sciences, California Institute of Technology, Pasadena, California 91125.

0019-1035/92 $5.00

sented by sections of spheres. That model and its applications are the subject of the present paper.

The model is simple enough that the solutions can be written in closed analytic form. By treating all the physics rigorously in this simple geometry, one gains insights that could otherwise be obtained only with a complete numerical model. That physics includes direct absorption of sunlight by the walls of the crater, scattering of sunlight and additional absorption within the crater, thermal emission by the walls, and scattering of emitted radiation and additional absorption. To get a simple solution, the surface must be a Lambert scatterer in both the visible and thermal infrared; i.e., the specific intensity of scattered and emitted radiation must be independent of direction. By assuming that each point on the inside of the crater is in radiative equilibrium, the temperature of the shadowed portions can be calculated exactly. A curious property of these solutions is that all shadowed portions of the crater are at the same temperature.

Adorjan (1970) and Hodges (1980) ignored multiple scattering, in effect assuming that the walls of the crater have zero albedo and unit emissivity. Although these are not bad assumptions for either the Moon or Mercury, a more complete treatment is possible. Possible applications include Mars and the icy satellites of the outer solar system, where scattering effects dominate. Following Svitek (1992), we consider multiple scattering of both visible and infrared radiation to all orders.

Verbiscer and Veverka (1990) have studied the scattering properties of natural snow and frost. They find strongly forward scattering phase functions, in contrast to the observed backscattering behavior of icy satellites (a Lambert surface scatters isotropically). They suggest that on icy satellites, frost grains are aggregated into particles of complex texture which produce the backscattering behavior. The difference probably depends on the temperature of the ice, and since Martian temperatures are intermediate between those on the Earth and the icy satellites, the Lambert scattering assumption is at least reasonable.

The model is described in Section 2. The approach is straightforward under the assumptions stated. We apply the model in Section 3 to the Moon and Mercury. We calculate the maximum temperatures of permanently shadowed areas using estimates of the depth/diameter ratios of typical lunar bowl-shaped craters (Pike, 1974, 1977) and assuming a saturated surface in which the craters are completely overlapping. We do not consider the important issues of the water abundance and supply rates or the lifetime of water in the atmosphere. For Mars (Section 4), we consider two cases: water frost in radiative equilibrium, and subliming CO_2 frost in vapor equilibrium—the difference being that longwave radiation is less important in the latter case. The question for Mars is "Will a depression lose material faster or slower than the surrounding flat surface?" When the answer is "faster," then the surface will become rougher, and vice versa.

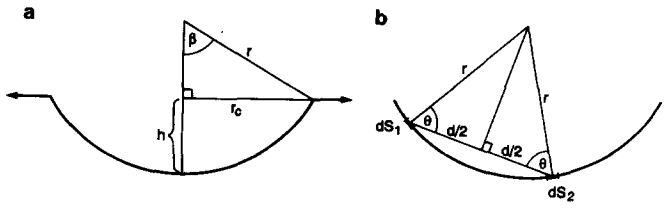

FIG. 1. (a) Cross-section in a vertical plane of a spherical bowl-shaped crater. The crater surface is a section of a sphere, whose center is the apex of the figure. The horizontal plane tangent to the rim of the crater is perpendicular to the page and is indicated by heavy arrows. (b) Typical scattering geometry in a plane containing the center of the sphere and two area elements dS_1 and dS_2, which are separated by a distance d. The vertical plane is not necessarily in the plane of the figure.

2. THE MODEL

The crater geometry is shown in Fig. 1a. The crater is a section of a sphere of radius r, with β the angle between the vertical and a line to the crater rim measured from the center of the sphere. The crater radius r_c, measured in the horizontal plane at the level of the crater rim, is therefore $r \sin \beta$. The crater depth h, which is the distance from this plane to the crater bottom, is $r(1 - \cos \beta)$. The diameter/depth ratio D is $2 \sin \beta/(1 - \cos \beta)$. The area of the crater in the horizontal plane is πr_c^2, and the spherical surface area S_c of the inside of the crater is $2\pi(1 - \cos \beta)r^2$. We define $f = S_c/4\pi r^2$, the ratio of the surface area of the inside of the crater to the surface area of the sphere. Useful relations are $f = (1 - \cos \beta)/2 = 1/(1 + D^2/4)$ and $\pi r_c^2/S_c = (1 - f)$.

Two surface elements of area dS_1 and dS_2 are shown in Fig. 1b. The plane of the paper contains both elements and the center of the sphere. The ray connecting the two elements has length d. The angle between the ray and the surface normal at S_1 and S_2 is Θ, so that $d = 2r \cos \Theta$. Thus $dS_1 \cos \Theta/d^2$ is the solid angle of element 1 as seen from element 2, and $dS_2 \cos \Theta$ is the surface area of element 2 projected onto a plane perpendicular to the ray from element 1. If I_1 is the specific intensity leaving element 1, then the contribution of element 1 to the power incident on element 2 is

$$dP = I_1 dS_1 dS_2 (\cos \Theta)^2/d^2.$$

Using the assumption of a Lambert surface, for which $I_1 = F_1/\pi$, and the relation $d = 2r \cos \Theta$, we obtain

$$dP = F_1 dS_1 dS_2/(4\pi r^2), \quad (1)$$

where F_1 is the power/area (flux) leaving the surface at S_1. This expression for dP is independent of the positions of the two elements and their relative distance. That is the important property of spherical Lambert surfaces that leads to analytic solutions.

We now apply Eq. (1) to the scattered sunlight and the scattered infrared emission to obtain the energy balance of the average surface element. Let $P(0)$ be the solar power incident on the crater, i.e.,

$$P(0) = F_0 \sin e_0 \pi r_c^2 = F_0 \sin e_0 (1 - f) S_c,$$

where F_0 is the solar constant (power/area) and e_0 is the solar elevation angle relative to the horizontal plane of the planet. A fraction $(1 - A)$ of this power is absorbed and a fraction A is scattered, where A is the visual albedo. This power, $P(0)A$, is scattered isotropically (according to a Lambert distribution) from the sunlit portions of the crater, and contributes to the power incident at the next order according to Eq. (1). Replacing $F_1 dS_1$ in Eq. (1) by $P(0)A$ is equivalent to integrating over the sunlit portions of the crater. Similarly, replacing dS_2 in Eq. (1) by S_c is equivalent to integrating over all elements on which the first-order scattered radiation is incident. Then using $f = S_c/4\pi r^2$, we find that $P(1)$, the total power incident anywhere within the crater after one scattering event, is

$$P(1) = P(0)Af.$$

The power goes down by a factor Af after each scattering event: the fraction directed back into the crater (not lost to space) is f and the fraction scattered is A, so a fraction Af remains. At the next order, a fraction $(1 - A)$ is absorbed and a fraction A is scattered. A similar argument yields

$$P(2) = P(1)Af = P(0)(Af)^2$$

for the power incident anywhere within the crater after two scattering events. The total power absorbed from solar radiation is then

$$(1 - A)[P(0) + P(1) + P(2) + \ldots] = P(0)\left[\frac{(1 - A)}{(1 - Af)}\right], \tag{2}$$

where the last step is obtained by summing the geometric series. The same expression minus the direct sunlight term $(1 - A)P(0)$ gives the power absorbed from scattered solar radiation:

$$(1 - A)[P(1) + P(2) + \ldots] = P(0)Af\left[\frac{(1 - A)}{(1 - Af)}\right]. \tag{3}$$

A similar analysis yields the total power absorbed from thermal radiation. Let E be the power emitted by all surface elements within the crater—the surface integral of $\varepsilon\sigma T^4$, where ε is the thermal emissivity and σ is the Stefan–Boltzmann constant. Thus

$$E = \varepsilon\langle\sigma T^4\rangle S_c,$$

where angular brackets denote an areal average over the walls of the crater. Replacing $F_1\, dS_1$ in Eq. (1) by E is equivalent to integrating over the emitting surface. Similarly, replacing dS_2 in Eq. (1) by S_c is equivalent to integrating over all elements on which emitted thermal radiation is incident. Then using $f = S_c/4\pi r^2$, we find that $E(0)$, the power incident anywhere within the crater from direct thermal radiation, is simply Ef. Of this, a fraction ε is absorbed and a fraction $(1 - \varepsilon)$ is scattered. This fraction becomes input to the next order of scattering, so that

$$E(1) = E(0)(1 - \varepsilon)f$$

is the longwave power incident anywhere within the crater after one scattering event, according to Eq. (1). Similarly we obtain

$$E(2) = E(1)(1 - \varepsilon)f = E(0)[(1 - \varepsilon)f]^2.$$

The total power absorbed from longwave radiation (not including the loss due to thermal emission) is then

$$\varepsilon[E(0) + E(1) + \ldots] = \frac{\varepsilon Ef}{[1 - (1 - \varepsilon)f]}. \tag{4}$$

Subtracting this from E yields the net power lost (emitted minus absorbed) at infrared wavelengths:

$$\frac{E(1 - f)}{[1 - (1 - \varepsilon)f]} = \frac{\varepsilon\langle\sigma T^4\rangle\pi r_c^2}{[1 - (1 - \varepsilon)f]}. \tag{5}$$

Equations (2) and (5) allow us to define the effective visual albedo and effective infrared emissivity of the crater, which is treated as a circular hole of radius r_c in the horizontal plane (see Fig. 1a). Dividing Eq. (2) by $P(0)$, the power incident on the crater/hole, we obtain

$$(1 - A_{\text{eff}}) = \frac{(1 - A)}{(1 - Af)} \tag{6}$$

as the ratio of power absorbed to power incident. For $f = 0$, which is a flat crater with depth/diameter = 0, the expression reduces to $(1 - A)$ and the effective visual albedo is A. For $f = 1$, which is a small hole in an otherwise

complete spherical cavity, the expression reduces to 1 and the effective visual albedo is zero.

The effective emissivity is obtained by dividing Eq. (5) by $\langle \sigma T^4 \rangle \pi r_c^2$, the power radiated by a blackbody of the same area as the crater/hole. Thus

$$\varepsilon_{\text{eff}} = \frac{\varepsilon}{[1 - (1 - \varepsilon)f]}. \tag{7}$$

For $f = 0$ (flat crater), this expression is just ε, which is the emissivity of the surface itself. And for $f = 1$ (small hole in an otherwise spherical cavity), the effective emissivity is unity.

Equations (2) and (5) give the total power in and the total power out, respectively. Equating them gives the value of E, and therefore of $\langle \sigma T^4 \rangle$, when the surface is in radiative equilibrium. The value of σT^4 for individual surface elements depends on whether or not they are in direct sunlight. For surfaces not in direct sunlight, the power/area (flux) absorbed from sunlight scattered off the walls of the crater is Eq. (3) divided by the area S_c. Equation (1) guarantees that all such surfaces absorb the same flux. The power/area absorbed from infrared radiation by the walls of the crater is Eq. (4) divided by the area S_c. In radiative equilibrium, the sum must be equal to the loss by direct thermal emission, $\varepsilon \sigma T^4$, so that

$$\sigma T^4 = F_0 \sin e_0 \frac{f(1 - A)}{(1 - Af)} \left[1 + \frac{A(1 - f)}{\varepsilon} \right]. \tag{8}$$

Equation (8) gives the equilibrium temperature of any element that is not in direct sunlight. All such elements have the same temperature, because they absorb the same flux according to Eq. (1). The terms Af and $A(1 - f)/\varepsilon$ arise from multiple scattering. Setting these terms to zero yields

$$\sigma T^4 = F_0 \sin e_0 (1 - A) f. \tag{9}$$

This is the same as Eq. (23) of Adorjan and Eq. (11) of Hodges, since f is $1/(1 + D^2/4)$, where D is the diameter/depth ratio. Equation (9) is rigorously valid only for $A = 0$. In that limit, it is valid for all ε, although the above authors restricted their derivations to $\varepsilon = 1$.

For small f (large diameter/depth ratio), Eq. (8) reduces to

$$\sigma T^4 = F_0 \sin e_0 \frac{4(1 - A)}{D^2} \left(1 + \frac{A}{\varepsilon} \right). \tag{10}$$

Equation (10) says that temperature decreases as the diameter/depth ratio D increases, as long as the crater is deep enough to have shadowed areas. The $1/D^2$ factor can be traced to the first factor of f that appears in Eqs. (3), (4), and (8). This factor arises because the shadowed elements of the crater warm each other. Although the flux (power/area) that any one element receives from any other element is independent of f according to Eq. (1), the flux that it receives from all other elements is proportional to their area and therefore to f. Greater input means greater output, so σT^4 is proportional to f.

For $f = 1$ (small hole in a closed spherical cavity), Eq. (8) reduces to $\sigma T^4 = F_0 \sin e_0$; i.e., the cavity acts like a blackbody in equilibrium with the incident sunlight. And Eq. (8) says that temperature increases as ε decreases, provided neither A nor $(1 - A)$ is zero, i.e., provided some light is scattered into the shadow and some fraction of that light is absorbed.

3. APPLICATION TO THE MOON AND MERCURY

The first application is to Mercury and the Moon. The reasoning is similar to that of Paige *et al.* (1992), but they focused only on Mercury. The goal is to use Eq. (8) to compute the temperatures in the shadowed portions of bowl-shaped craters at various distances from the pole. We then compute the maximum sublimation rate of a hypothetical frost at this temperature from simple kinetic theory.

We assume that the obliquity of Mercury is zero (Peale, 1988), so the Sun's center is always on the horizon at the poles of Mercury. Only the portion of the solar disk that is above the horizon is available to heat the crater. To find the effective value of $F_0 \sin e_0$, we integrate over the disk. Let r_s be the radius of the Sun and R be the distance to the target—a crater on the pole of Mercury. For a point on the solar disk, ρ is the apparent radial distance from the disk center, and λ is the azimuth around the disk starting from vertical—the perpendicular to the horizon at Mercury. Finally, $\phi = \arcsin(\rho/r_s)$ is colatitude from the line between the center of the Sun and the target.

Solar limb darkening is assumed to follow

$$I(\phi) = I(0)[(1 - u_1) + u_1 \cos \phi], \tag{11}$$

where I is specific intensity and u_1 is 0.54 (Allen, 1973). The solar constant F_0 at Mercury's distance is

$$F_0 = \int_0^{r_s} I(\rho) 2\pi\rho \, d\rho \, R^{-2}. \tag{12}$$

For $r_s \ll R$, the sine of the elevation angle of a point on the disk as seen from Mercury is $(\rho/R) \cos \lambda$, so the effective value of $\langle F_0 \sin e_0 \rangle$ is

$$\langle F_0 \sin e_0 \rangle = \int_0^{r_s} \int_{-\pi/2}^{+\pi/2} I(\rho) \cos \lambda \rho^2 d\rho \, R^{-3}. \quad (13)$$

With (11), the integrals in Eq. (12) and (13) yield

$$\langle \sin e_0 \rangle = \frac{\langle F_0 \sin e_0 \rangle}{F_0} = \frac{2r_s(1 - u_1 + 3\pi u_1/16)}{3\pi R(1 - u_1 + 2u_1/3)}. \quad (14)$$

The closest Mercury gets to the Sun is $a(1 - e)$, or 0.3075 AU, where a is the semimajor axis and e is the eccentricity. With these values, $\langle \sin e_0 \rangle$ is 3.046×10^{-3}, which is equivalent to a point source 0.1745° above the horizon.

Pike (1974, 1977) gives equations for the average depth/diameter ratios of fresh lunar craters. For diameters less than 15 km, the ratio is approximately 0.2. For diameters greater than 15 km, the ratio falls off as (diameter)$^{(-0.7)}$. Woronow *et al.* (1982) discuss the size–frequency distributions of craters on the Moon, Mercury, and Mars. They argue against saturation (complete coverage of the surface by craters of all sizes), even for the most heavily cratered terrains. Nevertheless, the curves they show are consistent with the view that each logarithmic interval in the crater diameter distribution contributes significantly to the areal coverage. For our purposes, the important point is that large fractions, 50% or more, of the heavily-cratered surfaces can be considered to be covered by bowl-shaped craters whose depth/diameter ratio is about 0.2. For such a crater the value of f is 0.1379.

Equation (8) allows us to compute the temperature in the shadowed areas of bowl-shaped craters at the poles of Mercury. With $\langle \sin e_0 \rangle = 3.046 \times 10^{-3}$, $R = 0.3075$ AU, $F_0 = (1370/R^2)$ W/m^2, $f = 0.1379$, $A = 0.068$, and $\varepsilon = 0.98$ (Allen, 1973), we obtain $T = 102$ K. At the pole, over half the area should be at or below this temperature, which applies to craters with depth/diameter ratios of 0.2 (and diameters less than 15 km according to Pike). Larger craters have smaller depth/diameter ratios and lower temperatures, although at normal incidence they cover a smaller fraction of the surface area. This result applies only at the exact pole ($e_0 < 0.1745°$, see above); what happens at other latitudes is discussed below. For these same values of $\langle \sin e_0 \rangle$, R, A, and ε, a flat horizontal surface has $T = 165$ K, in good agreement with the value quoted by Paige *et al.* (1992).

The above result allows us to assess the importance of internal heat flow, which we have neglected up to this point. The radiated flux from a 102 K black body is 6.1 W/m^2, which is 100 times greater than the average internal heat flow on Earth (Allen, 1973). If Mercury is similar to the Earth in this respect, the internal heat flux is negligible and we can safely assume radiative equilibrium for the shadowed areas. Internal heat flow becomes important at temperatures below 35 K, and could affect retention of volatiles other than water (Hodges 1980).

As shown by Watson *et al.* (1961), the rate of loss from ice on an otherwise airless body is greatest when the evaporating molecules are quickly removed from the body's atmosphere before they can recondense. Then the evaporation rate V from the ice is given by (Watson *et al.*, 1961)

$$V = \alpha P_s(T) \left(\frac{m}{2\pi kT}\right)^{1/2}, \quad (15)$$

where α is the sticking coefficient, P_s is the saturation vapor pressure, m is the molecular mass, and k is Boltzmann's constant. We choose $\alpha = 1.0$ and $P_s = B \exp(-C/T)$ with $B = 3.54 \times 10^{11}$ Pa and $C = 5737$ K (Bryson *et al.*, 1974). Taking the density of ice to be 0.9 g/cm^3, the maximum evaporation rate from ice at 102 K is 0.9 cm per 10^9 yr. This estimate is based on an extrapolation of the vapor pressure by more than five orders of magnitude, and could be wrong by a factor of 5. The important point is that the evaporation rate is extremely small at these temperatures. At these rates, even small deposits of ice will not evaporate in 10^9 years. For $T = 117$ K, the same formulas yield an evaporation rate of 10 m per 10^9 yr. A complete discussion of loss mechanisms other than evaporation is outside the scope of this paper.

The nonzero obliquity of the Moon and the precession of the orbit cause the selenographic latitude of the Sun to vary with a 347-day period (Astronomical Almanac, Section D). During this time the Sun rises once at each pole to an angle 1.6° above the horizon. The maximum value of $\sin e_0$ is then 2.792×10^{-2}, which is nine times greater than $\langle \sin e_0 \rangle$ at the poles of Mercury (note that $\langle \sin e_0 \rangle = \sin e_0$ when the Sun is entirely above the horizon). This factor of 9 almost compensates for the Moon's greater distance from the Sun, so that at $R = 0.981$ AU the yearly peak temperature in the shadowed portion of a polar lunar crater (depth/diameter = 0.2) is 99 K, which is close to that at Mercury.

The compensating factors apply only at the poles. Moving off the lunar pole by 1.6° doubles the value of $\sin e_0$, which increases the temperature by a factor of only 1.19. But moving off the pole of Mercury by the same amount increases the value of $\langle \sin e_0 \rangle$ from 3.046×10^{-3} to 2.792×10^{-2}, which increases the temperature by a factor of 1.74. If water were present on both objects, the latitudinal extent of the polar caps would be greater on the Moon. The radius of the heavily frosted area on Mercury, where ice fills the ubiquitous bowl-shaped craters with depth/diameter = 0.2, is only about 0.17° (7 km), which is the effective height of the Sun above the horizon as described earlier.

The above results are for craters with depth/diameter ratios of 0.2. Reducing the value of this ratio (reducing the

value of f) causes both the temperature of the shadowed portion and its fractional area to decrease (Hodges, 1980). For a given value of the solar elevation angle e_0, there is a value of f for which the shadows disappear. This limit is reached when β is equal to e_0, or $\cos e_0 = (1 - 2f)$ according to the relations accompanying Fig. 1a. Putting this formula into Eq. (8) with the value of T fixed, we can solve for the limiting values of f and e_0. The limiting e_0 is the highest solar elevation angle for which the temperatures of the shadowed areas are less than or equal to T. Temperatures this low will exist only for craters whose value of f satisfies the relation $\cos e_0 = (1 - 2f)$. This defines the limiting diameter/depth ratio D through the relation $f = 1/(1 + D^2/4)$. Such craters are as shallow as possible subject to the condition that they still have shadows.

For Mercury with $T = 102$ K, the limiting e_0 is 6.85° and the corresponding D is 33.4. For the Moon with $T = 102$ K, the limiting e_0 is 15.1° and the corresponding D is 15.1. Not surprisingly, the same temperature requires that the Sun be lower (closer to the horizon) on Mercury than on the Moon, which is partly compensated for by the larger allowed D for Mercury. Repeating the calculation for $T = 117$ K yields $e_0 = 8.2°$ ($D = 27.8$) for Mercury and $e_0 = 18.2°$ ($D = 12.5$) for the Moon. Only a small fraction of the surface will satisfy these conditions when the Sun is at its limiting elevation angle. Most of the craters will either be too shallow and have no shadows, or will be too deep and therefore too warm.

These values of e_0 are related to the latitudinal radii of any polar frost caps, should they exist. We shall define the cap radius as the maximum colatitude for which the temperatures in the shadowed areas are below the value $T = 102$ K. Because Mercury has no obliquity, the maximum colatitude is equal to the limiting value of e_0, or 6.85°. For high noon at lunar summer solstice, the maximum colatitude is the limiting value of e_0 minus 1.6°, or 13.5°. However, during the lunar day, additional portions of the crater will be illuminated. The colatitude for permanently shadowed areas on the Moon is a fraction of a degree less than the above value. The above estimates for Mercury are consistent with the half-power radius of 4° inferred from observations (Butler *et al.*, 1992).

4. POLAR FROSTS ON MARS

The other application is to the polar caps of Mars. We use the energy budgets and temperatures to determine whether a crater-like depression (cavity) loses mass (and grows in size) faster or slower than a flat horizontal surface. In a qualitative way, this tells whether the frost surface becomes rougher or smoother as it sublimes. Water frost is different from CO_2 frost because illuminated water frost is close to radiative equilibrium and CO_2 frost is close to vapor equilibrium. The relative importance of visible and infrared radiation is different for water frost and for rapidly subliming CO_2 frost. This leads to interesting differences in behavior.

For water, we assume radiative equilibrium and equate Eqs. (2) and (5). The result is

$$\varepsilon\langle\sigma T^4\rangle = F_0 \sin e_0(1 - A)\left[\frac{1 - (1 - \varepsilon)f}{(1 - Af)}\right], \quad (16)$$

where $\langle\sigma T^4\rangle$ is the area-weighted mean for the walls of the cavity. The quantity in square brackets is the ratio of $\langle\sigma T^4\rangle$ inside the cavity to σT^4 outside it. As long as $(1 - \varepsilon) < A$, the mean temperatures will be higher within the cavity and the walls will lose mass faster than the horizontal surface. The cavity will grow in volume, although it will not maintain its spherical shape; the parts of the cavity that are in direct sunlight will be the warmest and they will grow the fastest. Our prediction is that a water surface will become rough on Mars. Thus, the north residual water ice cap and that part of the south residual cap composed of water ice should be rough by our analysis. Svitek (1992) develops this concept further by analogy with sublimation-dominated ice features on Earth.

For CO_2, we assume $T = 148$ K = constant. The evaporation rate is proportional to the net (visible minus infrared) energy flux. For a cavity, this is the difference between Eqs. (2) and (5) divided by S_c. The result is

$$(1 - f)\left\{\frac{F_0 \sin e_0(1 - A)}{(1 - Af)} - \frac{\varepsilon\sigma T^4}{[1 - (1 - \varepsilon)f]}\right\} = F_c, \quad (17)$$

where F_c is the mean power/area absorbed by the walls of the cavity. This is compared to

$$F_0 \sin e_0(1 - A) - \varepsilon\sigma T^4 = F_h, \quad (18)$$

where F_h is the power/area absorbed by the horizontal surface. The neutral curves, for which $F_c = F_h$, are plotted in Fig. 2 assuming Mars to be 1.525 AU from the Sun. The curves show the values where $F_c = F_h$ for finite f (cavities neither open nor closed). The region above and to the left of the $f = 0$ curve has F_h greater than F_c for all finite f. The horizontal surface evaporates faster, and the average surface becomes smoother (f approaches 0). The region below and to the right of the $f = 1$ curve has F_c greater than F_h for all $f < 1$, so the average surface becomes rougher (the model implies f would increase toward 1, but in reality the cavity would lose its spherical shape before reaching that value; our model treats only the average energy inputs to the walls of the cavity, and neglects

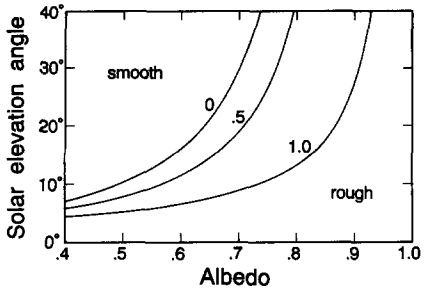

FIG. 2. Roughness of subliming CO_2 on Mars. The curves are labeled by the value of f, which is the ratio of the surface area of the cavity to the surface area of the sphere. Large f means that the cavities are well-developed and the surface is rough. Small f means that the cavities are flat and the surface is smooth. For each point between the curves $f = 0$ and $f = 1$ there is a value of f for which the crater surface and the horizontal surface are losing mass at the same rate. Outside this range the rates are different. For small solar elevation angles (lower right portion of the figure), the crater surface loses mass faster and the average surface becomes rougher. For large solar elevation angles (upper left portion of the figure) and $f > 0$, the horizontal surface loses mass faster and the average surface becomes smoother.

differences between the portions in sunlight and those in shadow).

Small e_0 favors a rough surface. In this case, subliming CO_2 is like water ice; absorbed sunlight is comparable to infrared emission, and the cavity grows. The opposite (high Sun) case favors a smooth surface; absorption of sunlight dominates, and because the absorbed energy is spread over a larger area inside the cavity than outside it, the cavity loses mass more slowly than the horizontal surface. Although our model holds strictly for spherical bowl-shaped cavities and does not account for the change in shape as the cavity sublimes, we use it here to make a few speculative remarks about CO_2 on Mars.

The dividing line between rough and smooth surfaces (Fig. 2) is an interesting one for Mars. At the poles the solar elevation angle e_0 is 25° at the time of summer solstice. At other seasons, e_0 is smaller. Also, the albedo of the frost is in the range 0.55 to 0.75 (Paige and Ingersoll, 1985), so the surface roughness could go either way. If subliming CO_2 does become smoother as the solar elevation angle increases (or as Mars moves closer to the Sun—the two are equivalent in this model), then the effective albedo would increase (Eq. (6) as $f \rightarrow 0$). This behavior of subliming CO_2 frost could explain a puzzling difference between the north and south polar caps of Mars—the systematically higher apparent albedoes at summer solstice in the south (Paige, 1985; Paige and Ingersoll, 1985). Because perihelion occurs near southern summer solstice, the southern cap receives more power/area (insolation) than the north and therefore should have a higher albedo according to our speculation. This is a fundamental difference (Paige, 1985), because it may help explain why only the southern CO_2 frost cap can survive the summer—it absorbs less energy because of its higher albedo.

To get some idea of the magnitude of the effect, consider a hypothetical surface whose albedo is 0.75 when there are no cavities. Then cover the surface with cavities of all sizes and of hemispheric cross section ($f = 0.5$). The effective albedo drops to 0.6, according to Eq. (6), provided the cavities are nested so that the surface is all cavities. This change in albedo, from 0.75 to 0.6, is comparable to the difference between the south polar cap at maximum insolation and the north or south cap at lower insolation (Paige, 1985; Paige and Ingersoll, 1985). We emphasize that our results are based on the average energy inputs to spherical bowl-shaped cavities. The portions of the cavities that are in direct sunlight will lose mass faster than average, so it is not clear the CO_2 frost on Mars will ever become perfectly smooth, even in the low-albedo high-Sun case. Also, our discussion assumes that the frost is thicker than the roughness elements. For CO_2 at the north pole, this may not be such a good assumption. There the thickness is of order 1 m, which is characteristic of the annual frost deposits. Roughness elements larger than this thickness will "bottom out." Smaller elements will become smoother because of thermal conduction within the frost. Certainly at the south pole, the frost should be thick enough to become rough by repeated sublimation of seasonal layers.

Colwell *et al.* (1990) arrived at much the same conclusions in their study of the evolution of topography (icy craters and trenches) on comets. They found, using a numerical model, an enhancement in the net sublimation rate for trenches and craters farther from the Sun than some critical distance. This is equivalent to our finding that the subliming CO_2 becomes rougher at low insolation. Colwell *et al.* also find that craters and trenches close to the Sun have a lower sublimation rate than the surrounding terrain, which is equivalent to our statement that the surface becomes smoother at high insolation rates.

Roughness is a measurable quantity, independent of the albedo. It should be possible, using the angular distribution of scattered visible radiation and emitted thermal radiation, to determine whether the south CO_2 cap has a higher albedo because it is smoother or because it is less dusty. Hapke (1984), for example, treats the effects of macroscopic roughness on the angular scattering properties of surfaces. Generally, rough surfaces scatter more in the backward direction than smooth surfaces, and the thermal emission may be more sharply peaked toward the Sun than away from it. The effect is more pronounced for low-albedo surfaces than for high-albedo surfaces. Further work is needed to quantify the effect and determine how best to measure it from Mars Observer.

ACKNOWLEDGMENTS

We acknowledge helpful discussions and comments by Bryan Butler (California Institute of Technology), Bruce Jakosky (University of Colorado), and David Paige (University of California, Los Angeles) during early stages of this paper. This research was supported in part by NASA's Planetary Atmospheres Program under Grant NAGW-1956 and by NASA Grant NAGW-1373.

REFERENCES

ADORJAN, A. S. (1970). Temperature distribution in shadowed lunar craters. *J. Spacecraft* **7,** 378–380.

ALLEN, C. W. (1973). *Astrophysical Quantities*. Athlone, London, and Dover, New Hampshire.

BRYSON, C. E., III, V. CAZCARRA, AND L. L. LEVENSON (1974). Sublimation rates and vapor pressures of H_2O, CO_2, N_2O, and Xe, *J. Chem. Eng. Data* **19,** 107–110.

BUTLER, B., D. O. MUHLEMAN, AND M. A. SLADE (1992). Mercury: Full disk radar images, and the detection and stability of ice at the North Pole. Submitted for publication.

COLWELL, J. E., B. M. JAKOSKY, B. J. SANDOR, AND S. A. STERN (1990). Evolution of topography on comets. II. Icy craters and trenches. *Icarus* **85,** 205–215.

HAPKE, B. (1984). Bidirectional reflectance spectroscopy. *Icarus* **59,** 41–59.

HARMON, J. K., AND M. A. SLADE (1992). Radar mapping of Mercury: Full-disk delay-doppler images. Submitted for publication.

HODGES, R. R., JR. (1980). Lunar cold traps and their influence on argon-40. In *Proc. Lunar Planet. Sci. Conf. 11,* pp. 2463–2477.

PAIGE, D. A. (1985). *The Annual Heat Balance of the Martian Polar Caps from Viking Observations*. Ph.D. Thesis, California Institute of Technology.

PAIGE, D. A., AND A. P. INGERSOLL (1985). Annual heat balance of martian polar caps: Viking observations. *Science* **228,** 1160–1168.

PAIGE, D. A., S. E. WOOD, AND A. R. VASAVADA (1992). The thermal stability of water ice at the poles of Mercury. Submitted for publication.

PEALE, S. J. (1988). The rotational dynamics of Mercury and the state of its core. In *Mercury* (F. Villas, C. R. Chapman, and M. S. Matthews, Eds.), pp. 461–493. Univ. of Arizona Press, Tucson.

PIKE, R. J. (1974). Depth/diameter relations of fresh lunar craters: Revision from spacecraft data. *Geophys. Res. Lett.* **1,** 291–294.

PIKE, R. J. (1977). Size-dependence in the shape of fresh impact craters on the Moon. In *Impact and Explosion Cratering* (D. J. Roddy, R. O. Pepin, and R. B. Merrill, Eds.), pp. 489–509. Pergamon, New York.

SLADE, M. A., B. J. BUTLER AND D. O. MUHLEMAN (1992). Mercury radar imaging, evidence for polar ice. Submitted for publication.

SVITEK, T. (1992). *Martian Water Frost: Control of Global Distribution by Small-scale Processes*. Ph.D. Thesis, California Institute of Technology, Pasadena, CA.

VERBISCER, A. J., AND J. VEVERKA (1990). Scattering properties of natural snow and frost: Comparison with icy satellite photometry. *Icarus* **88,** 418–428.

WATSON, K., B. C. MURRAY, AND H. BROWN (1961). The behavior of volatiles on the lunar surface. *J. Geophys. Res.* **66,** 3033–3045.

WORONOW, A., R. G. STROM, AND M. GURNIS (1982). Interpreting the cratering record: Mercury to Ganymede and Callisto. In *Satellites of Jupiter* (D. Morrison, Ed.), pp. 237–276. Univ. of Arizona Press, Tucson.